Steel and Composite Structures, *Vol. 23, No. 4 (2017) 483-491*
DOI: https://doi.org/10.12989/scs.2017.23.4.483

Experimental study on concrete-encased composite columns with separate steel sections

Congzhen Xiao [1a], Fei Deng [*2], Tao Chen [1] and Zuozhou Zhao [2]

[1] *China Academy of Building Research, 30 Beisanhuandong Lu, Beijing, China*
[2] *Department of Civil Engineering, Tsinghua University, 30 Shuangqing Lu, Beijing, China*

(*Received November 19, 2015, Revised January 14, 2017, Accepted January 22, 2017*)

Abstract. This paper presents an experimental study on the behavior of concrete-encased composite columns with multi-separate steel sections subjected to axial and eccentric loads. Six 1/4-scaled concrete-encased composite columns were tested under static loads. The specimens were identical in geometric dimensions and configurations, and the parameter of this experiment was the eccentricity ratio of the applied load. Each two of the specimens were loaded with 0, 10%, and 15% eccentricity ratios. The capacity, deformation pattern, and failure mode of the specimens were carefully examined. Test results indicate that full composite action between the concrete and the steel sections can be realized even though the steel sections do not connect with one another. The concrete-encased composite columns can develop stable behavior and sufficient deformation capacity by providing enough transverse reinforcing bars. Capacities of the specimens were evaluated based on both the Plain Section Assumption (PSA) method and the superimposition method. Results show that U.S. and Chinese codes can be accurate and safe in terms of bending capacities. Test results also indicate that the ACI 318 and Mirza methods give the best predictions on the flexural stiffness of this kind of composite columns.

Keywords: static test; concrete-encased composite column; separate steel sections; capacity; stiffness

1. Introduction

Composite columns are frequently used in high-rise buildings. Compared to reinforced concrete (RC) columns, composite columns often provide a higher bearing capacity and ductility without significantly enlarging the dimensions of the column (Morino 1998, Roeder 1998). Two commonly used types of composite columns are concrete-encased composite columns and concrete-filled steel tube columns. The concrete-encased composite column contains a structural steel with or without shear connectors and the surrounding concrete which is further reinforced by longitudinal bars and transverse bars. By utilizing the composite action between the concrete and the steel section, the capacity of the composite column is higher than the summation of the capacities of the concrete and the steel section (Ye *et al.* 2000).

A great amount of experiments have been conducted to study the behavior of concrete-encased composite columns subjected to axial and eccentric loads (Oh *et al.* 2006), cyclic loads (Ricles and Paboojian 1994, El-Tawil and Deierlein 1999, Shim *et al.* 2011, Naito *et al* 2010), and biaxial loads (Munoz and Hsu 1997, Tokgoz and Dundar 2008, Dundar *et al.* 2008). Specimens with high-strength steel shapes and concrete were also studied (Kim *et al.* 2011, 2013). Most of the studies were focused on the capacity and ductility of the composite columns. In addition, composite columns with T-shaped and L-shaped steel sections (Chen *et al.* 2005, Tokgoz and Dundar 2012) and new types of spirals (Weng *et al.* 2008) were tested. The results revealed that the concrete-encased composite columns showed favorable seismic performance and ductility if the concrete could be properly confined.

As the height of the high-rise buildings further increases, the dimensions of the composite columns have to be enlarged to carry the gravity loads and to provide enough lateral stiffness. By replacing the single built-up steel section with several smaller but separate rolled shapes (Fig. 1), a considerable amount of welding work can be saved in

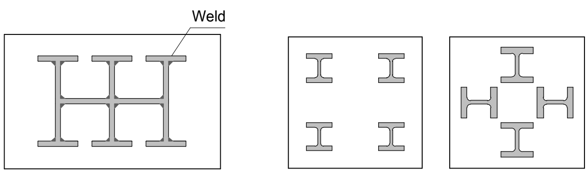

(a) Column with a single steel section
(b) Column with multi-separate steel sections

Fig. 1 Different types of composite columns

*Corresponding author, Ph.D. Candidate,
E-mail: dengf13@mails.tsinghua.edu.cn
[a] Research Fellow, Ph.D.,
E-mail: xiaocongzhen@cabrtech.com

http://www.techno-press.org/?journal=scs&subpage=6
ISSN: 1229-9367 (Print), 1598-6233 (Online)

situ, thus reducing the cost and increasing the return on investment of the project. However, limited experiments have been conducted to study the behavior of concrete-encased composite columns with multi-separate steel sections. Current code provisions provide a variety of approaches to determine the capacity of concrete-encased composite columns under combined compression and bending, such as ACI 318 (2008), AISC-LRFD (2016), and YB 9082 (2006). However, these code provisions do not provide approaches to determine the capacity of concrete-encased composite columns with multi-separate steel sections.

This study tries to provide an insight into the behavior of concrete-encased composite columns with multi-separate steel sections. Six 1/4-scaled specimens were tested under static axial and eccentric loads. The primary objective of this study is to examine the behavior and capacity of the composite columns. In addition, an evaluation on the current ACI 318, AISC-LRFD, and YB 9082 code provisions is presented by comparing the code predictions with test results.

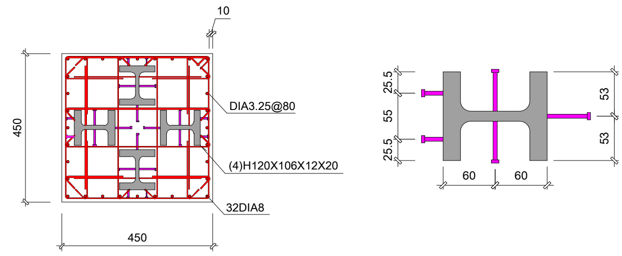

(a) Cross section configuration (b) Shear studs

Fig. 2 The cross-section of the specimen

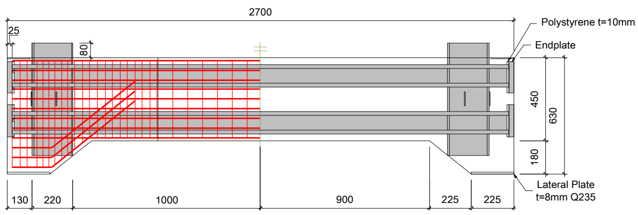

Fig. 3 Details and dimensions of the specimen

2. Experimental program

2.1 Specimen design

Six identical specimens were designed in this test program based on a super high-rise building in China. The scaling factor of the specimens was taken as 1/4 considering the capacity of the testing machines. The major parameter in this test program was the eccentricity ratio e/h, where e was the eccentricity of the applied load, and h was the width of the composite cross section. Every two of the specimens were loaded under the same eccentricity ratio. Specifically, specimen E00-1 and E00-2 were loaded with $e/h = 0$; E10-1 and E10-2 with $e/h = 10\%$; and E15-1 and E15-2 with $e/h = 15\%$.

The dimension of the cross section was 450 × 450 mm. Four I-shaped hot rolled steel sections with dimensions of 120 × 106 × 12 × 20 mm were encased in the concrete. Each of the steel sections was located on one side of the composite column, and the distance between the center of the steel sections and the center of the cross section was 137.5 mm. Shear studs were provided on the surfaces of the steel sections. The diameter and length of the shear studs were 6 mm and 50 mm, respectively. Since the edges of the steel sections were very close to the boundary of the cross section, shear studs that were placed on the outside of the steel sections were cut to 25-mm long to ensure enough thickness of the concrete cover. The interval of the shear studs in the longitudinal direction was 144 mm. The longitudinal reinforcement was provided by 8-mm diameter deformed bars, and the transverse reinforcement was provided by 3.25-mm diameter iron wires with intervals of 80 mm. Note that some of the transverse reinforcing bars were intersecting with the webs of the steel sections. In this case, each of the transverse reinforcing bars was cut into two segments, and each of the segments was welded on the web of the steel section. Details of the cross section are presented in Fig. 2.

Fig. 3 shows the overall dimensions of the specimen. The length of the column was 2700 mm, and each end of the column had a bracket for applying the eccentric load. Two I-shaped steel beams were installed at each end of the column to simulate the beam-column joint, and dimensions of the in-plane and out-of-plane steel beams were 220 × 110 × 5.9 × 9.2 mm and 140 × 73 × 4.7 × 6.9 mm, respectively. To ensure safety and to prevent premature failure during the test, the ends of the specimens were confined by 8-mm thick steel plates. Since the least favorable cross section was in the middle of the specimen, the steel plates would have little influence on the capacity of the composite columns.

2.2 Test setup and loading protocol

The experiment was conducted in Tsinghua University with a servo-controlled testing machine whose maximum capacity was 20000 kN. As shown in Fig. 4, each end of the specimen was encased into a steel cap for further confinement, and every steel cap was connected to a hinge that could only rotate in-plane. One of the hinges was placed on the ground, and was fixed by two blocks to avoid any horizontal displacement. While the other one was installed on the top of the specimen, connecting to the transition beam. The transition beam was connected to two horizontal actuators on both sides, whose purpose was to prevent lateral displacement of the transition beam. During the test, the displacement of the horizontal actuators was strictly controlled to ensure that the transition beam did not move horizontally.

Note that a 10-mm thick layer of sand was placed at each end of the specimen between the surface of the specimen and the steel cap. Since the sand was soft, the constraint between the steel sections and the concrete was released. Namely, the surfaces of the steel sections and the concrete would not be forced into the same plane, thus providing more appropriate boundary conditions. However, the axial load carried by the concrete and the steel sections

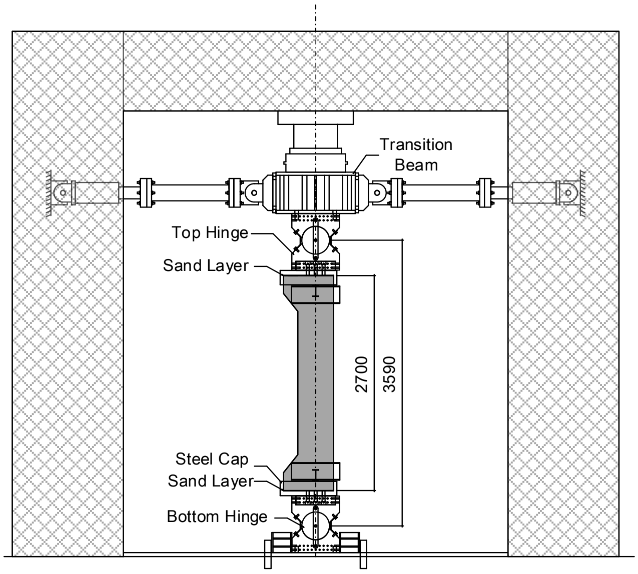

Fig. 4 Test setup

would be influenced due to the existence of the sand. Therefore, a steel endplate was installed at each end of the steel sections to correct the axial load carried by the steel sections and the concrete. The area of the endplate was specially designed to make sure that the compressive strain of the concrete and the steel sections were the same on the surface of the column. If the sand and the endplates were not provided, the following equations can be obtained

$$\varepsilon_s = \varepsilon_c \tag{1}$$

$$\frac{N_s}{E_s A_s} = \frac{N_c}{E_c A_c} \quad \text{or} \quad \frac{N_s}{N_c} = \frac{E_s A_s}{E_c A_c} \tag{2}$$

$$\frac{N_s}{N_c + N_s} = \frac{E_s A_s}{E_c A_c + E_s A_s} \tag{3}$$

where ε, A, E, and N are the compressive strain, cross area, modulus of elasticity, and the axial force; the subscript 'c' and 's' identify the concrete and steel sections, respectively. Assume the pressure was uniformly distributed in the sand. Consequently, the ratio of N_s to N_0 was proportional to the ratio of A_{ep} to A_0, where N_0 and A_0 are the axial force and cross area of the entire cross section, and A_{ep} is the sum of the area of the endplates. Based on Eq. (3), the following equation can be obtained.

$$A_{ep} = \frac{E_s A_s}{E_c A_c + E_s A_s} A_0 \tag{4}$$

The area of the endplates could be determined by Eq. (4). In addition, the centroid of every endplate coincided with the centroid of the corresponding steel section to avoid local bending of the steel section (Fig. 5).

Note that a piece of 10-mm thick polystyrene, whose purpose was the same as the sand layer, was also installed beneath each endplate before the concrete was placed. The sand, the endplates, and the polystyrene worked together to make the boundary conditions as accurate as possible.

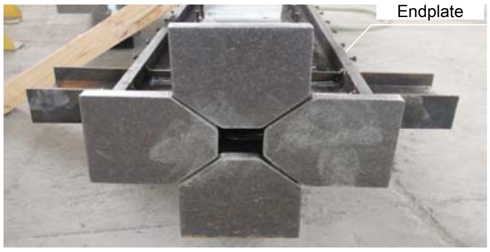

Fig. 5 The endplates

Table 1 Material properties

Specimen	f_{cu} /MPa	f_y/MPa			
		Flange	Web	Longitudinal bars	Transverse bars
E00-1	61.2	408	523	438	597
E00-2	56.6	398	411		
E10-1	60.9	423	435		
E10-2	72.8	383	415		
E15-1	66.1	377	404		
E15-2	67.6	389	405		
AVE	64.8	396	432	438	597

*f_{cu} = concrete compressive strength, f_y = steel yield strength

The axial load was applied by the vertical actuator at a very slow rate. Experimental data were collected during the test, including the axial load, the vertical deflection of the column, the lateral deflection of the mid-height cross section, and the strain of the steel sections and the concrete on the mid-height cross section. The tests were stopped when the concrete was severely damaged.

2.3 Material properties

The columns were made of C60 concrete, and the size of the aggregate was carefully controlled to fit the scaled specimens. The concrete was placed in winter with the environment temperature ranging from 10°C~15°C. The concrete compressive strength was obtained from 150 × 150 × 150 mm blocks which were tested on the same day the corresponding specimen was tested. The steel sections and beams were hot rolled shapes made of S355 and S235 steel, respectively. Tested material properties are listed in Table 1.

3. Experimental results and discussions

3.1 General behaviors

<u>*Specimen E00-1/E00-2*</u>

Specimen E00-1 and E00-2 were loaded with *e/h* = 0. Since the behavior of these two specimens were very similar, specimen E00-1 is used as an example for description. A vertical crack was observed on the face of the

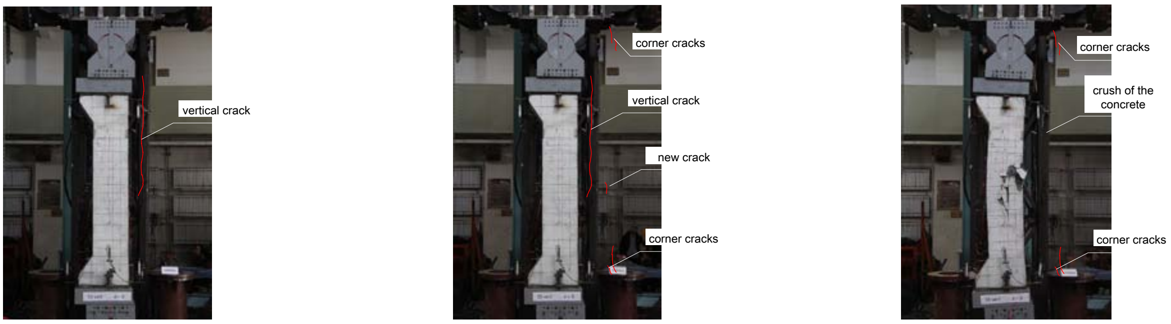

(a) 70% of the maximum load (b) After the maximum load (c) Failure mode

Fig. 6 Crack distribution of specimen E00-1

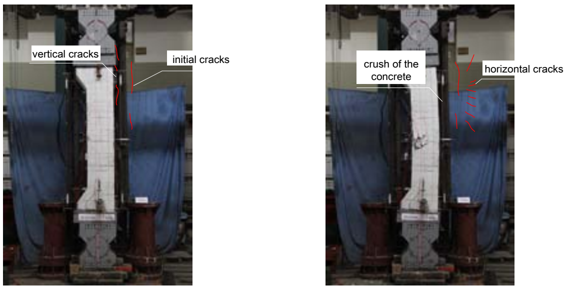

(a) 70% of the maximum load (b) Failure mode

Fig. 7 Crack distribution of specimen E10-1

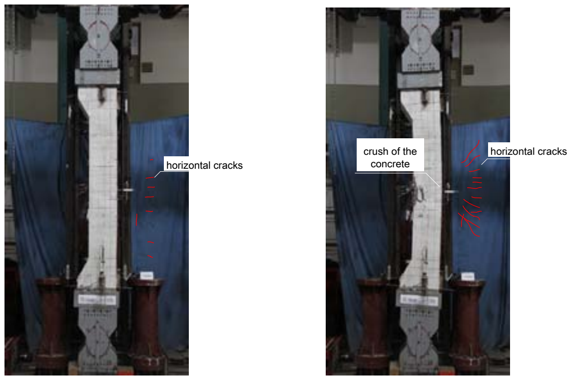

(a) 70% of the maximum load (b) Failure mode

Fig. 8 Crack distribution of specimen E15-1

specimen when the axial load reached about 50% of the maximum load. The length of the crack grew as the load increased, but no extra cracks occurred. When the axial load reached 70% of the maximum load, the initial crack stopped growing and ended up in a longitudinal crack in the middle of the column (Fig. 6(a)). In fact, the concrete cover at the middle of the column was very thin due to the existence of the steel sections. Therefore, this part of the concrete was weaker than the others, which led to the longitudinal cracking under axial load. In addition, the splitting effect caused by the shear studs might also contribute to the cracking of the concrete.

No significant deformations were observed before the maximum axial load was reached. As the test went on, a new vertical crack occurred near the initial one, but did not develop much (Fig. 6(b)). Then, the axial load dropped suddenly accompanied by cracking of the concrete at the corners of the column after the maximum axial load was reached. The cracking of the concrete corners resulted in rotation of the column ends, which led to lateral deflection of the column. Therefore, the second order bending moment developed on the mid-height cross section of the column. As the test went on, the vertical deflection of the column developed rapidly and the axial load gradually decreased. Finally, the column failed due to the crush of the concrete in the middle (Fig. 6(c)).

Specimen E10-1/E10-2

Specimen E10-1 failed in combined compression and bending pattern. Similar to specimen E00-1, initial longitudinal cracks were observed in the middle of specimen E10-1 when the axial load reached 50% of the maximum load. Soon after, a few vertical cracks occurred on the compression side of the column, and the cracks kept growing as the test went on (Fig. 7(a)). Since the eccentricity ratio was small for specimen E10-1, no horizontal cracks were observed before the maximum load was reached.

The horizontal deflection of the column developed rapidly after the maximum load was reached, so the actual eccentricity ratio on the mid-height cross section was enlarged due to the second order effect, and horizontal cracks occurred on the tension side of the column. Meanwhile, damage of the concrete on the compression side of the column kept developing. In the end, the test was stopped when the concrete on the compression side was severely damaged (Fig. 7(b)).

Specimen E15-1/E15-2

Specimen E15-1 and E15-2 also failed in combined compression and bending pattern. However, since the eccentricity ratios of E15-1&E15-2 were larger than that of E10-1&E10-2, horizontal cracks occurred on the tension

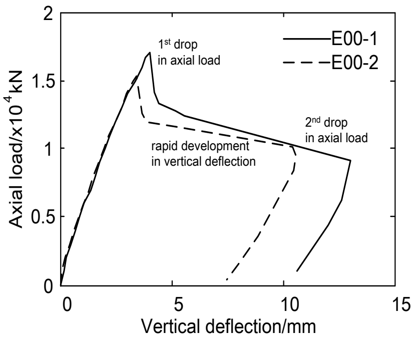

(a) Specimen E00-1&E00-2

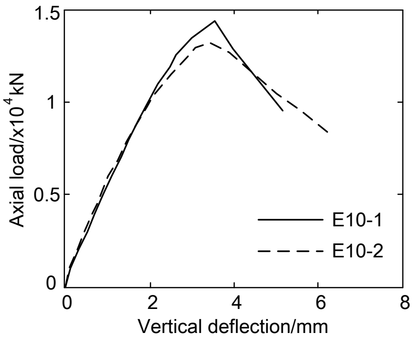

(b) Specimen E10-1&E10-2

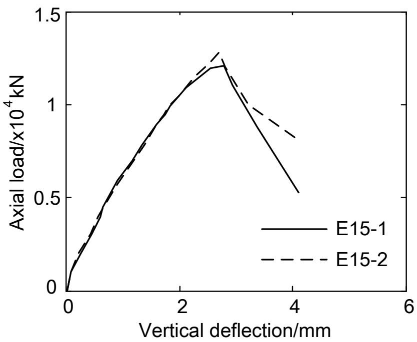

(c) Specimen E15-1&E15-2

Fig. 9 Load-vertical deflection curves

side of the column before vertical cracks occurred on the compression side of the column. Damage of the concrete on the compression side was not observed until the maximum load was reached. Similarly, a considerable amount of horizontal cracks and crush of the concrete were observed when the specimen failed.

3.2 Capacities of the specimens

The axial load - vertical deflection curves of the specimens are presented in Fig. 9. As mentioned above, the axial load of specimen E00-1 and E00-2 showed two sudden drops during the test. The first drop occurred right after the maximum load was reached, and the axial load dropped to 70% of the maximum. Then, the axial load gradually decreased from 70% to 60% of the maximum load, while the vertical deflection was developing rapidly. When the axial load had decreased to about 60% of the maximum load, the second drop in axial load occurred, accompanied by the sudden crush of the concrete in the middle of the column. On the other hand, no sudden drops in axial load were detected for the eccentrically loaded specimens. After the maximum loads were reached, the axial loads of these four specimens gradually decreased until failure.

Table 2 lists the capacities and the corresponding bending moments on the mid-height cross section of the columns. The bending moment was determined as follows

$$M = N(e_i + \delta) \quad (5)$$

where e_i is the initial eccentricity of the specimen, and δ is the horizontal deflection of the mid-height cross section due to the second order effect. Although the initial eccentricity of specimen E00-1 and E00-2 was zero, horizontal deflections of these two columns were recorded during the test. Nevertheless, the eccentricities were very small under the maximum load level, so that the axial resistances of these two specimens were not significantly influenced.

For specimens subjected to eccentric loads, the eccentricities under the maximum load level were 19% ~ 33% larger than the initial eccentricities due to the second order effect. Since this paper deals with short columns, the second order effect will not be discussed in details.

Table 2 Capacities of the specimens

Specimen	$N_{\max}$ /kN	M /kNm	Eccentricity ratio	$e_{\text{failure}}/e_{\text{initial}}$
E00-1	17082	143	1.9%	-
E00-2	15325	52	0.8%	-
E10-1	14360	803	12.4%	1.24
E10-2	13231	767	12.9%	1.29
E15-1	12041	1076	19.9%	1.33
E15-2	12759	1026	17.9%	1.19

3.3 Strain distributions

The normal strain of the steel sections and the concrete were recorded during the test. The layout of the strain gauges on the mid-height cross section is presented in Fig. 10. Specifically, four strain gauges were installed on steel section 1# and 4#, and three were installed on steel section 2# and 3#. The surfaces of the column were also installed with strain gauges as shown in Fig. 10.

Specimen E10-1 was chosen as an example to illustrate the strain distribution of the specimens. Shown in Fig. 11(a) are the strain distributions of the concrete and the steel sections under four load levels: load levels corresponding to 20%, 60%, and 100% of the maximum load, and the failure load level. Test results indicate that the entire mid-height cross section was in compression before the maximum load

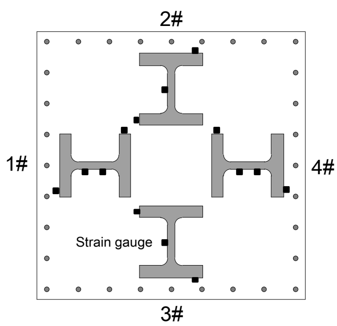

(a) Steel sections

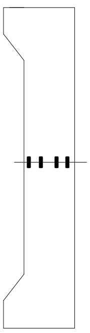
(b) Concrete

Fig. 10 Layout of strain gauges

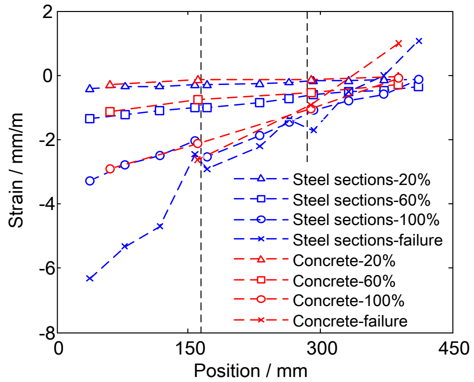

(a) Strain distribution of concrete and steel sections

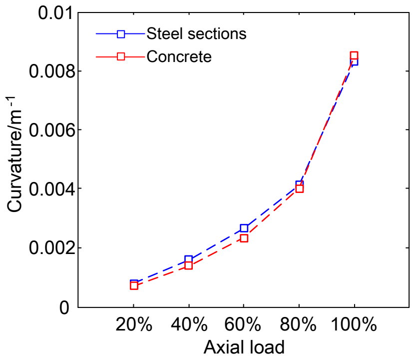

(b) Curvature of concrete and steel sections

Fig. 11 Strain distribution and curvature of E10-1

was reached, and that tensile stress occurred under the failure load level. It is clear that the cross section almost remained plane up to the maximum load level. Although the strain distributions of the steel sections and the concrete were nonlinear under the failure load level, it did not significantly violate the plane section assumption.

Based on the least square method, a linear regression of the normal strains on the positions of the strain gauges was established to find the curvature of the mid-height cross section. In this way, the slope of the regressed line could be taken as the curvature of the cross section, which can be mathematically expressed as follows

$$\mathrm{Curvature} = \frac{\mathrm{Cov}(x, \varepsilon)}{\mathrm{Var}(x)} \tag{6}$$

where x is the position of the strain gauge, and ε is the strain. Fig. 11(b) presents the relationship between the curvature and the load level for the steel sections and the concrete, which further supports the effectiveness of the plane section assumption.

4. Evaluations on current code provisions

4.1 Flexural resistance

In general, flexural capacities of composite members can be determined by two methods – the Plane Section Assumption (PSA) method and the superimposition method, of which the former one is adopted by US codes ACI 318 (2008) and AISC-LRFD (2016), and the latter one by Japanese code AIJ-SRC (1991) *AIJ standards for structural calculation of steel reinforced concrete structures* and Chinese code YB 9082 (2006) *Technical Specification of Steel-Reinforced Concrete Structures*.

For PSA method, the following assumptions are adopted:

(1) Plane sections remain plane;
(2) Full composite action between the concrete and the steel sections can be achieved up to failure of the composite member;
(3) The stress distribution of the concrete is simplified as an equivalent rectangular diagram;
(4) The tensile strength of the concrete is often neglected.

Specifically, in ACI 318, the coefficient of 0.85 is applied to concrete compressive strength. Given an axial load, the corresponding flexural capacity of the composite member can be obtained based on the plastic stress distribution on the composite cross-section, and the interaction curve can be then obtained. Furthermore, the design axial strength of composite members are limited to 80% of the nominal axial strength of the composite members with tie reinforcement to account for the minimum eccentricity.

Similar to ACI 318, the axial and pure flexural resistance of the composite member can also be obtained according to the PSA method in AISC-LRFD code. However, the interaction curve is calculated based on the following equations

$$\text{For } \frac{P_u}{\phi P_n} \geq 0.2, \quad \frac{P_u}{\phi P_n} + \frac{8}{9}\frac{M_u}{\phi_b M_n} \leq 1.0 \tag{7a}$$

$$\text{For } \frac{P_u}{\phi P_n} < 0.2, \quad \frac{P_u}{2\phi P_n} + \frac{\mathrm{M_u}}{\phi_\mathrm{b} \mathrm{M_n}} \leq 1.0 \tag{7b}$$

where P_n and M_n are the nominal axial and pure flexural capacity of the composite member, respectively; P_u and M_u are the axial load and corresponding flexural capacity of the composite member, respectively; and ϕ is a reduction factor. Therefore, the interaction curve given by AISC-LRFD is a bilinear line instead of a curve.

The superimposition method is adopted by AIJ-SRC to calculate the flexural capacity of composite members. In this method, the axial load is divided into two parts carried by steel and reinforced concrete, respectively. The flexural capacity of each component is calculated based on the axial load carried by itself, and the flexural capacity of the composite member can be obtained by adding that of each component. However, the calculated flexural capacity is affected by how to divide the axial load. Among all the methods to divide the axial load, the one that creates the maximum flexural capacity is the one that corresponds to PSA method. AIJ-SRC provides two simplified methods to divide the axial load. In the first one, the axial load is carried by reinforced concrete prior. If the axial load is larger than the axial resistance of the reinforced concrete part, the exceeding proportion will be carried by the structural steel. The second method is on the contrary.

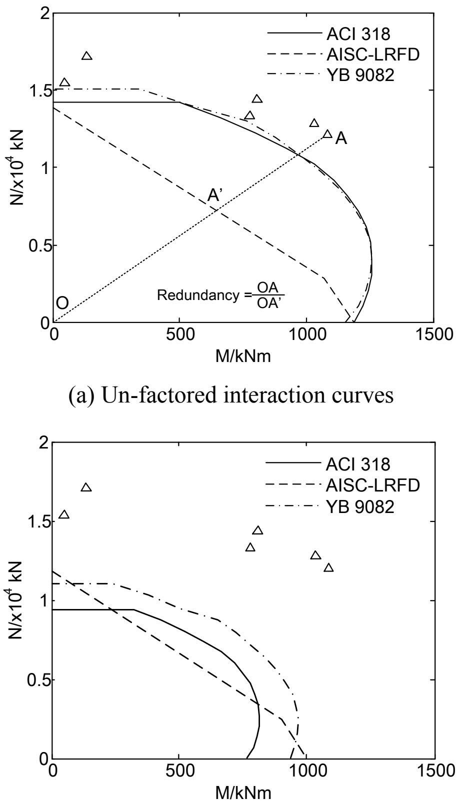

(a) Un-factored interaction curves

(b) Factored interaction curves

Fig. 12 Code predictions on the flexural capacity

However, these simplified methods may make the calculations much conservative. Therefore, a more reasonable method is proposed in YB 9082 to divide the axial load

$$N_{cy}^{ss} = \frac{N - N_b}{N_{u0} - N_b} N_{c0}^{ss} \tag{8a}$$

$$M_{cy}^{ss} = \left(1 - \left|\frac{N_{cy}^{ss}}{N_{c0}^{ss}}\right|^m\right) M_{y0}^{ss} \tag{8b}$$

where N_{cy}^{ss} and M_{cy}^{ss} are the axial load carried by the structural steel and its corresponding flexural capacity; N_{u0} is the axial resistance of the composite corss-section; N_{c0}^{ss} is the axial resistance of the structural steel; N_b is the axial load corresponding to balance conditions; and M_{y0}^{ss} is the pure flexural capacity of the structural steel.

Predictions provided by these codes are presented in Fig. 12(a) together with the test results. To evaluate the code provisions, the redundancy factor is defined as follows:

(1) Draw a straight line between the origin and the test result;
(2) The redundancy factor is defined as the ratio of the distance between the origin and the test result to the distance between the origin and the intersection of the straight line and the interaction curve (Fig. 12(a)).

The ACI 318 and YB 9082 yield similar results, while the AISC-LRFD provides more conservative results. Specifically, the average redundancy factors for ACI 318, AISC-LRFD, and YB 9082 are 1.12, 1.50, and 1.08, respectively. However, this does not necessarily mean that the AISC-LRFD provides the most conservative results in the design of concrete-encased composite columns, since the strength reduction factors have not been included so far.

ACI 318 specifies that the ϕ factor to be taken as 0.65 for compression-controlled sections with tie reinforcement, and that the ϕ factor is permitted to increase linearly from 0.65 to 0.90 as the net tensile strain in the extreme tension steel at nominal strength increases from the compression-controlled strain limit to 0.005. The ϕ factor specified by AISC-LRFD is 0.85 for axial strength. For flexural strength, the ϕ factor is also taken as 0.85 if the nominal flexural strength is determined based on the plastic stress distribution of the composite cross section (If other design philosophies are adopted, the ϕ factor can be different). Chinese codes do not apply the strength reduction factors to the calculated strength of the cross section. Rather, the strength reduction factors are applied to the material strength. According to Chinese codes (GB50010 2010, GB50017 2003), the factored strength of the material is the characteristic value of the material strength divided by γ_R. The values of γ_R for concrete, reinforcing bars, and steel sections are 1.40, 1.10, and 1.11 respectively.

Fig. 12(b) shows the interaction curves with the strength reduction factors included. Diversities of the test results come from diversities in material properties, applied loads, boundary conditions, and measurement errors. When the strength reduction factors or partial safety factors are not considered, the code predictions are all on the safe side. This is mainly because the confinement effect was not considered when evaluating the compressive strength of the concrete. Threfore, ACI 318 and YB 9082 underestimate the test results by giving slightly larger un-factored capacities. The AISC-LRFD is too conservative because a bilinear line is used to construct the interaction curve. Compared to un-factored capacities, redundancy factors for factored capacities provided by the three codes are closer to each other, especially for AISC-LRFD. Fig. 12(b) reveals that ACI 318 is more conservative than YB 9082 under any circumstances. Compared to AISC-LRFD, ACI 318 is more conservative when the axial strength is very large or very small, but is less conservative in the middle part of the

Table 3 Code predictions

Specimen	N_{test} /kN	M_{test} /kNm	Un-factored			Factored		
			ACI	AISC	YB9082	ACI	AISC	YB9082
E00-1	17082	143	1.09	1.16	1.01	1.61	1.30	1.37
E00-2	15325	52	1.20	1.34	1.14	1.77	1.54	1.54
E10-1	14360	803	1.12	1.62	1.09	1.68	1.88	1.49
E10-2	13231	767	1.06	1.53	1.01	1.56	1.78	1.41
E15-1	12041	1076	1.12	1.66	1.12	1.69	1.91	1.47
E15-2	12759	1026	1.13	1.69	1.13	1.72	1.94	1.49
Average			1.12	1.50	1.08	1.67	1.72	1.46
COV			0.002	0.044	0.003	0.005	0.065	0.004

interaction curves. The average redundancy factors for ACI 318, AISC-LRFD, and YB 9082 are 1.67, 1.72, and 1.46, respectively (see Table 3).

However, it should be noted that the redundancy factors do NOT reflect the safety margins in the real project, since the load factors and other related design specifications have not been included yet, which is beyond the scope of this paper.

4.2 Effective flexural stiffness

Most of the codes permit to determine the second order bending moment of a column based on the first order linear analysis of the structure using the effective flexural stiffness of the columns. According to Mirza and Tikka (1999), the effective flexural stiffness of a composite member subjected to compression and bending can be determined as follows

$$EI_{eff} = \frac{PL^2}{4\left(sec^{-1}\frac{M_s}{M_c}\right)^2} \tag{9}$$

where P is the axial load of the column at failure load level; L is the net length of the column; M_s and M_c are the bending moments at the center and end of the column at load level P, respectively. (Kim *et al.* 2011, 2013). Eqs. 10(a)~(d) list the specified effective flexural stiffness provided by ACI 318 , ANSI/AISC , GB 50010 , and Mirza, respectively

$$EI_{eff}^{ACI} = 0.2E_cI_g + E_{ss}I_{ss} \tag{10a}$$

$$EI_{eff}^{ANSI} = c_1E_cI_c + E_{ss}I_{ss} + 0.5E_rI_r \tag{10b}$$

$$EI_{eff}^{GB} = 0.6E_cI_c + E_{ss}I_{ss} \tag{10c}$$

$$\begin{aligned} EI_{eff}^{Mirza} &= (0.313 + 0.00334\frac{L}{H} + 0.203\frac{e}{H})E_cI_c \\ &+0.792E_{ss}I_{ss} + 0.788E_rI_r \end{aligned} \tag{10d}$$

where E_cI_c, $E_{ss}I_{ss}$, and E_rI_r are the bending stiffness for concrete, steel sections, and reinforcing bars, respectively; e is the eccentricity of the axial load; L and H are the length and width of the composite column. An important difference among these methods is that the ANSI/AISC and Mirza methods take into account the contribution of reinforcing bars, while the ACI 318 and GB 50010 methods do not. In addition, in Mirza method, the load eccentricity and slenderness of the column is considered to determine the stiffness reduction factor of the concrete. Also, Mirza method applies the 0.792 stiffness reduction factor to the steel sections, but the other three codes do not.

The calculated results are presented in Table 4, where the ratio of predicted EI_{eff} to tested EI_{eff} are listed in the brackets. According to the test results, the effective flexural stiffness of the composite columns decrease as the eccentricity ratios increase. This is because the larger eccentricity ratio induces more horizontal cracks in the tension zone of the concrete, hence reducing the stiffness of the column. However, the code provisions do not include the influence of the eccentricity ratio. In general, the ACI 318 and Mirza methods provide best predictions on the flexural stiffness of the specimens. Compared to ACI 318, the stiffness reduction factor for concrete is relatively larger in Mirza method, but the factor for steel sections is smaller. As a result, the calculated results provided by these two methods are similar. The ANSI/AISC method slightly overestimates the effective flexural stiffness of the column when the eccentricity ratio grows to 15%. The GB 50010 method overestimates the effective flexural stiffness significantly, because the reduction factor for concrete is too large in this standard.

Table 4 Effective flexural stiffness /kN·m^2

	E10-1	E10-2	E15-1	E15-2
Test	120708	90846	78169	80153
ACI 318	73058 (0.61)	73728 (0.81)	73667 (0.94)	74165 (0.93)
ANSI/AISC	81023 (0.67)	82025 (0.90)	81932 (1.05)	82679 (1.03)
GB 50010	104969 (0.87)	106738 (1.17)	106572 (1.36)	107890 (1.35)
Mirza and Tikka (1999)	73212 (0.61)	74160 (0.82)	72913 (0.93)	73596 (0.92)

5. Conclusions

Six 1/4-scaled concrete-encased composite columns with multi-separate steel sections were tested. All of the specimens failed in combined compression and bending patterns under axial and eccentric loads. Test results indicate that full composite action between the concrete and the steel sections can be realized up to failure. Plane sections remain plane during the test.

The code provisions in ACI 318, AISC-LRFD, and YB 9082 may provide accurate predictions on the axial and flexural capacity of the specimens with rational redundancy factors.

The ACI 318 and Mirza methods give the best predictions on the effective flexural stiffness of the composite columns. When the eccentricity ratio is large (15%), the ANSI/AISC overestimates the test results. While the GB 50010 overestimates the test results no matter what the eccentricity ratio is.

Acknowledgments

The authors gratefully acknowledge the financial support of ArcelorMittal. Contributions from Council on Tall Buildings and Urban Habitat (CTBUH) and Magnusson Klemencic Associates (MKA) are also appreciated.

References

ACI 318 (2008), Building code requirements for structural concrete and commentary; American Concrete Institute;

Farmington Hills, MI, USA.
AISC-LRFD (2016), Load and resistance factor design specifications for structural steel buildings; American Institute of Steel Construction; Chicago, IL, USA.
ANSI/AISC (2010), Specification for structural steel buildings, American Institute of Steel Construction; Chicago, IL, USA.
AIJ-SRC (1991), AIJ standards for structural calculation of steel reinforced concrete structures; Architectural Institute of Japan; Tokyo, Japan.
Chen, C.C., Li, J.M. and Weng, C.C, (2005), "Experimental behaviour and strength of concrete-encased composite beam–columns with T-shaped steel section under cyclic loading", *J. Constr. Steel Res.*, **61**(7), 863-881.
Dundar, C., Tokgoz, S., Tanrikulu, A.K. and Baran, T. (2008), "Behaviour of reinforced and concrete-encased composite columns subjected to biaxial bending and axial load", *Build. Environ.*, **43**(6), 1109-1120.
El-Tawil, S. and Deierlein, G.G. (1999), "Strength and ductility of concrete encased composite columns", *J. Struct. Eng.*, **125**(9), 1009-1019.
GB 50010 (2010), Code for design of concrete structures; Ministry of Housing and Urban-Rural Development of China; Beijing, China.
GB 50017 (2003), Code for design of steel structures; Ministry of Housing and Urban-Rural Development of China; Beijing, China.
Kim, C.S., Park, H.G., Chung, K.S. and Choi, I.R. (2011), "Eccentric axial load testing for concrete-encased steel columns using 800 MPa steel and 100 MPa concrete", *J. Struct. Eng.*, **138**(8), 1019-1031.
Kim, C.S., Park, H.G., Chung, K.S. and Choi, I.R. (2013), "Eccentric axial load capacity of high-strength steel-concrete composite columns of various sectional shapes", *J. Struct. Eng.*, **140**(4), 04013091.
Mirza, S.A. and Tikka, T.K. (1999), "Flexural stiffness of composite columns subjected to major axis bending", *ACI Struct. J.*, **96**(1), 19-28.
Morino, S. (1998), "Recent developments in hybrid structures in Japan—research, design and construction", *Eng. Struct.*, **20**(4), 336-346.
Munoz, P.R. and Hsu, C.T.T. (1997), "Behavior of biaxially loaded concrete-encased composite columns", *J. Struct. Eng.*, **123**(9), 1163-1171.
Naito, H., Akiyama, M. and Suzuki, M. (2010), "Ductility evaluation of concrete-encased steel bridge piers subjected to lateral cyclic loading", *J. Bridge Eng.*, **16**(1), 72-81.
Oh, M.H., Ju, Y.K., Kim, M.H. and Kim, S.D. (2006), "Structural performance of steel-concrete composite column subjected to axial and flexural loading", *J. Asian Architect. Build. Eng.*, **5**(1), 153-160.
Roeder, C.W. (1998), "Overview of hybrid and composite systems for seismic design in the United States", *Eng. Struct.*, **20**(4), 355-363.
Ricles, J.M. and Paboojian, S.D. (1994), "Seismic performance of steel-encased composite columns", *J. Struct. Eng.*, **120**(8), 2474-2494.
Shim, C.S., Chung, Y.S. and Yoon, J.Y. (2011), "Cyclic behavior of prefabricated circular composite columns with low steel ratio", *Eng. Struct.*, **33**(9), 2525-2534.
Tokgoz, S. and Dundar, C. (2008), "Experimental tests on biaxially loaded concrete-encased composite columns", *Steel Compos. Struct., Int. J.*, **8**(5), 423-438.
Tokgoz, S. and Dundar, C. (2012), "Tests of eccentrically loaded L-shaped section steel fiber high strength reinforced concrete and composite columns", *Eng. Struct.*, **38**(4), 134-141.
Weng, C., Yin, Y., Wang, J. and Liang, C. (2008), "Seismic cyclic loading test of SRC columns confined with 5-spirals", *Science in China Series E: Technological Sciences*, **51**(5), 529-555.
YB 9082 (2006), Technical specification of steel-reinforced concrete structures; Ministry of Housing and Urban-Rural Development of China; Beijing, China.
Ye, L. and Ehua, F. (2000), "State-of-the-art of study on the behaviors of steel reinforced concrete structure", *China Civil Eng. J.*, **33**(5), 1-11.

CC